JACS
JOURNAL OF THE AMERICAN CHEMICAL SOCIETY

Article

pubs.acs.org/JACS

Allosterically Controlled Threading of Polymers through Macrocyclic Dimers

Seda Cantekin,*[,†] Albert J. Markvoort,[‡] Johannes A. A. W. Elemans,[†] Alan E. Rowan,[†] and Roeland J. M. Nolte*[,†]

[†]Institute for Molecules and Materials, Radboud University Nijmegen, Heyendaalseweg 135, 6525 AJ, Nijmegen, The Netherlands

[‡]Institute for Complex Molecular Systems and Computational Biology Group, Eindhoven University of Technology, P.O. Box 513, 5600 MB Eindhoven, The Netherlands

Supporting Information

ABSTRACT: As part of an ongoing study to construct a molecular Turing machine in which a polymer chain is encoded via allosteric information transfer between macrocyclic complexes, we describe the thermodynamic and kinetic characterization of a multicomponent self-assembled system based on a zinc porphyrin macrocyclic compound, a bidentate ligand (1,4-diazabicyclo[2.2.2]octane, DABCO), and a viologen-substituted polymer guest. Initial addition of DABCO to the porphyrin macrocycle in chloroform solution leads to the formation of a stable 2:1 (porphyrin:DABCO) dimeric complex, even under dilute conditions, by means of strong cooperative interactions involving hydrogen and metal−ligand bonds. Further titration of the porphyrin-DABCO mixtures with the polymer gives rise to a complex array of species in the solution. The system is analyzed in detail by a combination of spectroscopic measurements and computational modeling. Each association constant in the binding scheme and the fraction of each individual complex that is formed in solution are determined precisely using a mass-balance model. Kinetic studies revealed that the rates of the polymer threading and dethreading in and out of the dimeric system are remarkably slow, indicating that the polymer is locked inside the cavity of the stable 2:1 dimeric complex as a result of strong allosteric interactions.

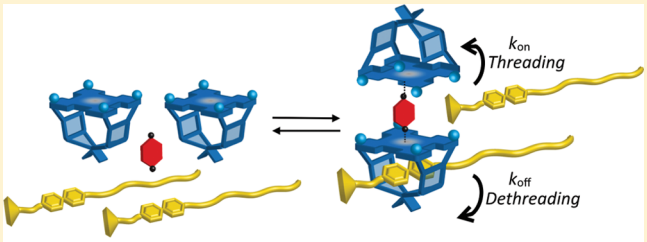

Multicomponent self-assembly leads to slow (de)threading rates

INTRODUCTION

Cooperative effects that are observed in the binding of two or more substrates to different binding sites of a receptor as a result of a conformational change caused by the binding of the first substrate are called allosteric interactions.[1] Allosteric regulation is a widely observed mechanism in biological systems and is used to control the function of proteins and enzymes in cellular metabolism. The application of cooperative interactions as used by nature to construct multicomponent self-assembled systems and to control functions such as molecular recognition, signal amplification, reactivity, and catalysis has been an intriguing field of research for organic and bio-organic chemists.[1−8] Over the years, various multicomponent systems displaying positive[9−12] and negative[13−15] homotropic[16] and heterotropic[17,18] cooperative binding phenomena have been developed. In these systems, the binding affinity of one component to one site can affect the affinity of the other site by means of steric, conformational, or electrostatic communication.[19] In order to be able to mimic the processes observed in complex enzyme systems (e.g., information transfer in DNA replication) with these synthetic supramolecular models, the nature of the interactions between the individual components in the synthetic multicomponent assemblies should be understood; the fraction of possible complexes formed, as well as the kinetic and thermodynamic parameters of the system, should be quantified accurately. We previously reported on a simple and efficient procedure for deriving cooperative binding effects from experimentally obtained kinetic and thermodynamic data, which can be used as a guide to study synthetic and natural cooperative binding systems.[20] Furthermore, we showed that the binding affinity of a guest can be enhanced by means of allosteric interactions in a multicomponent self-assembled system based on a combination of host−guest and metal−ligand interactions.[21] This previously described system consisted of a cavity-appended zinc porphyrin host and various combinations of ligands and substrates such as 4-*tert*-butylpyridine, 1,4-diazabicyclo[2.2.2]octane (DABCO), and dimethylviologen. In this synthetic system the binding affinity of DABCO to the zinc porphyrin host was enhanced in the presence of a viologen guest in the cavity, which resulted in the formation of a 1:1:1 complex (macrocycle:DABCO:viologen); however, the equilibrium of a double-decker complex with two macrocycles assembled by DABCO and viologen (macrocycle:viologen:DABCO:macrocycle:viologen; pentameric complex) was not directed to full assembly, as a result of negative cooperative effects.[21] Further studies revealed, however, that in the presence of stabilizing hydrogen bonding

Received: January 14, 2015
Published: March 3, 2015

DOI: 10.1021/jacs.5b00431
J. Am. Chem. Soc. 2015, 137, 3915−3923

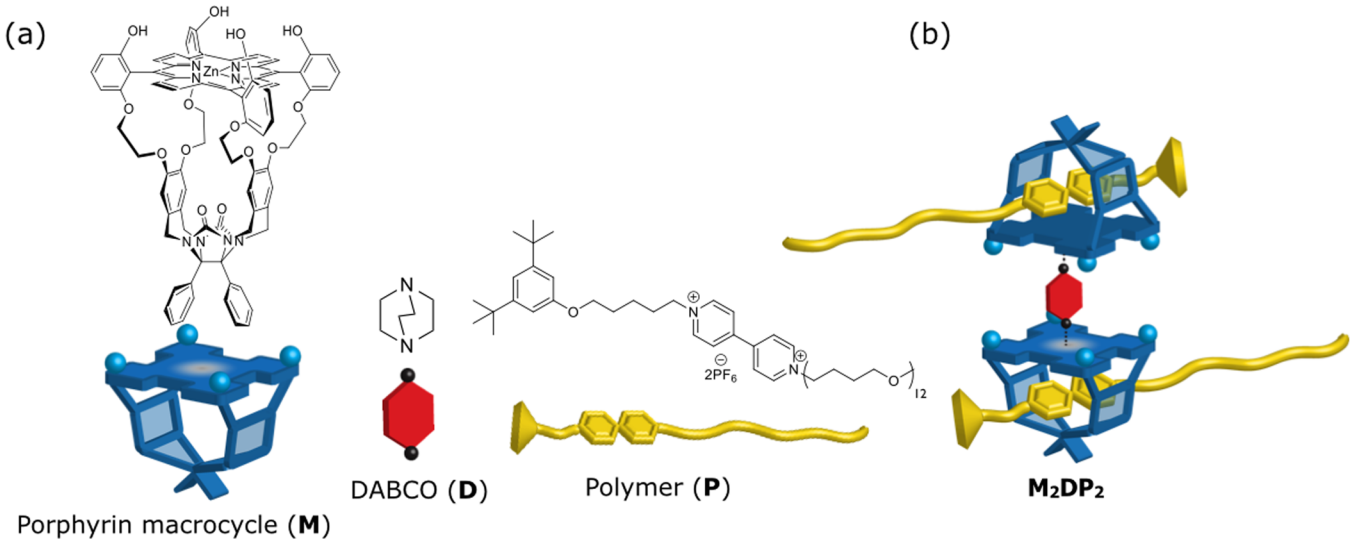

Figure 1. (a) Chemical structures of the compounds and the corresponding cartoons: Zn-tetrahydroxy-porphyrin macrocycle (**M**), DABCO ligand (**D**), and viologen-functionalized polytetrahydrofuran polymer (**P**). (b) Schematic representation of the pentameric complex ($\mathbf{M_2DP_2}$).

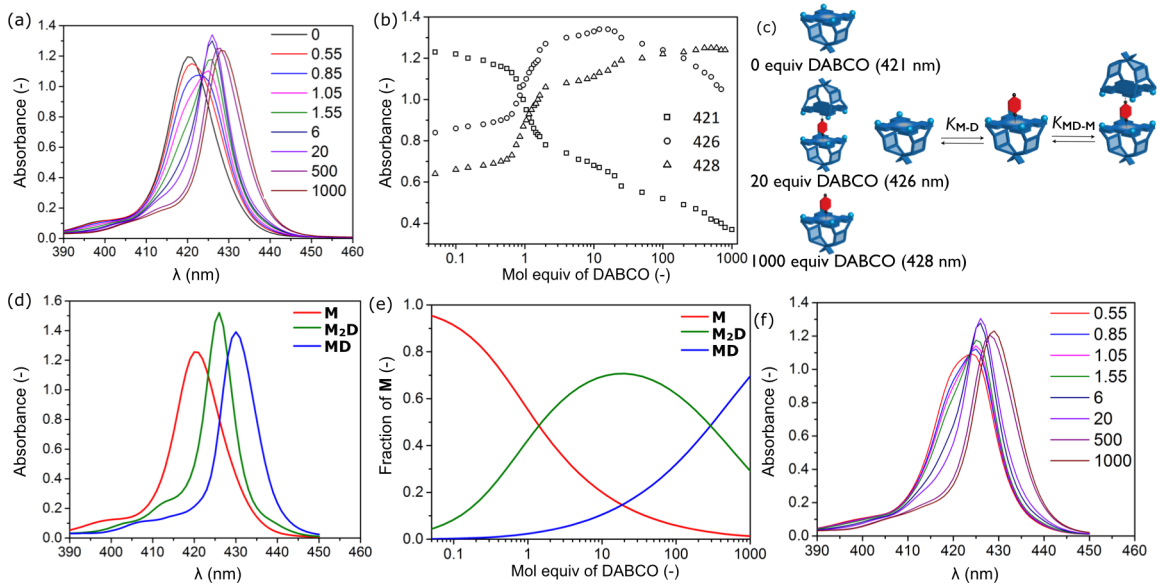

Figure 2. Titration of macrocycle **M** with **D** in $CHCl_3$ ([**M**] = 5.5 μM). (a) Selected UV−vis spectra during the course of the titration. Mol equiv of **D** are indicated (see Supporting Information Figure S3a for the complete set of spectra). (b) Change in UV−vis absorbance of **M** at three different wavelengths (421, 426, 428 nm) as a function of mol equiv of DABCO. (c) Schematic representation of the three species formed as a result of binding of **D** to **M** and the binding scheme. (d) UV−vis spectra of the individual species extracted from the experimental data using the mass-balance model. (e) Fraction of the macrocycle as **M** unbound to DABCO and as a component in $\mathbf{M_2D}$ and **MD** as a function of mol equiv of DABCO obtained from the fit. (f) Reconstructed UV−vis spectra based on (d) and (e); the fractions were computed using the optimized values of $K_{\text{M-D}} = 1 \times 10^4$ M^{-1} and $K_{\text{MD-M}} = 3 \times 10^6$ M^{-1} (see Supporting Information Figure S8b for the complete set of spectra).

hydroxyl groups on the porphyrin roof of the host, the two cage compounds self-assembled much more favorably into the above-mentioned pentameric complex, which was formed nearly quantitatively when sufficiently high concentrations of macrocycle, DABCO and viologen were used (~1 mM).

The present work is aimed at constructing a molecular Turing machine, which consists of a catalytically active double-cage system.[22] In this system, information is written (i.e., chemical modification of the polymer chain takes place) on a polymeric chain threaded through one of the cages and the instructions are obtained from the other cage by means of cooperative and allosteric interactions. In order to be able to construct such a machine, we here study the binding behavior and threading kinetics of a viologen-substituted polytetrahydrofuran (polyTHF) polymer (**P**) through a dimeric system based on Zn-tetrahydroxy-porphyrin macrocycle (**M**) and the ligand DABCO (**D**) (Figure 1a). A stable 2:1 (porphyrin:DABCO) dimeric complex is formed when DABCO is added to a dilute zinc porphyrin macrocycle solution, as a result of cooperative hydrogen bonding and metal−ligand interactions. The binding affinity of the viologen-substituted polymer inside of the cavity is enhanced in the presence of the ligand DABCO as a result of allosteric interactions. Consequently, even in dilute solutions a large fraction of a pentameric complex, which is needed for the information transfer, is formed (Figure 1b). We quantify the fraction of each

DOI: 10.1021/jacs.5b00431
J. Am. Chem. Soc. 2015, 137, 3915−3923

species that is present in the solution as well as the corresponding association constants by using a mass-balance method. This methodology allows us to extract distinct spectral data of the individual species from overlapping UV−vis and fluorescence emission spectra. Analysis of the dethreading and threading kinetics revealed that the enhanced binding affinity of the polymer inside the cavity leads to changes in the kinetics of polymer threading. A remarkably slow dethreading rate of the polymer from one of the cages in the pentameric complex is observed, indicating that the complex is held together by means of strong allosteric interactions and that the polymers are locked in the cavities of the self-assembled complex. In addition, the reverse process, i.e., the threading of one polymer through the unoccupied cage, while the other cage is already occupied by another polymer, is also very slow. This suggests that the open end of the first binding polymer chain interferes with the unoccupied cavity and delays the threading of the second polymer. The study represented here shows that even in dilute solutions information transfer is possible between two cage molecules and is expressed by means of allosteric interactions.

RESULTS AND DISCUSSION

Thermodynamics of Polymer Threading through Macrocyclic Dimers. Macrocycle **M** and viologen-functionalized polymer **P** were synthesized according to a previously published procedure with slight modifications[14,23,24] (see Supporting Information Section 2). The binding of DABCO **D** and polymer **P** to **M** was studied by UV−vis and fluorescence spectroscopy in dilute chloroform solution. The UV−vis spectrum of the macrocycle **M** shows a Soret band (λ_{max}) at 421 nm ([**M**] = 5.5 μM, Figure 2a, black line). The absorption spectrum of **M** displays a broader band compared to that of the previously studied zinc porphyrin macrocycle without OH groups[25] (see Supporting Information Figure S2), which is presumably the result of hydrogen-bonding effects in dilute chloroform solution. The initial addition of DABCO (0.55−20 mol equiv) to a solution of **M** in $CHCl_3$ resulted in a red shift of the λ_{max} from 421 to 426 nm (Figure 2a, see Supporting Information Figure S3a for the complete spectra). Upon further addition of DABCO (500−1000 mol equiv) the intensity of the band at 426 nm decreased and a new band appeared at 428 nm. The gradual red shift of the λ_{max} is characteristic for the formation of 2:1 and 1:1 porphyrin-DABCO complexes, as was previously reported.[19,26−29] Therefore, the three distinct peaks in the UV−vis spectra of **M** and DABCO mixture are assigned to three species: free macrocycle **M** (λ_{max} = 421 nm), $\mathbf{M_2D}$ complex (λ_{max} = 426 nm), and **MD** complex (λ_{max} = 428 nm). Similar titration experiments performed under identical conditions by using the monodentate ligand 4-*tert*-butylpyridine and **M** did not result in a similar gradual red shift in the UV−vis spectra of **M**. On the contrary, the absorption spectra displayed a sharp transition from 421 to 428 nm upon addition of 4-*tert*-butylpyridine, which indicates that only the expected 1:1 complex is formed (see Supporting Information Figure S3b). Furthermore, the UV−vis spectra of the zinc porphyrin macrocycle without the OH groups in chloroform showed a similar sharp transition upon the addition of DABCO, indicating the formation of only a 1:1 complex in the absence of hydrogen-bonding interactions (see Supporting Information Figure S3c). Figure 2b shows the complexation isotherms for **M** and DABCO at three different wavelengths. This figure suggests that upon the addition of DABCO the concentration of free macrocycle **M** decreases (squares), while the concentration of $\mathbf{M_2D}$ (circles) and **MD** (triangles) increases. Finally, in the presence of excess DABCO the concentration of $\mathbf{M_2D}$ decreases again, while the concentration of **MD** further increases. Figure 2a,b also illustrates that the two equilibria take place simultaneously and that the UV−vis absorption bands of **M**, **MD**, and $\mathbf{M_2D}$ overlap. Therefore, the abundance ratio of the species cannot be determined simply from the maximum absorbance values at individual wavelengths. Instead, we extracted the spectra of the individual species from the measured spectra using a mass-balance model. In our model, we assumed that only **M**, **MD**, and $\mathbf{M_2D}$ are present in the solution and that the concentration of the species formed is determined by two association constants, $K_{M\text{-}D}$ and $K_{MD\text{-}M}$ (Figure 2c). For given values of these association constants, the fractions of the macrocycle present as free **M** and as a component in **MD** and $\mathbf{M_2D}$ complexes were calculated for different DABCO concentrations (see Supporting Information Sections 5 and 6). Given these fractions and the experimental UV−vis spectra for solutions containing three different DABCO concentrations, one can calculate which unique combination of the spectra for the three individual species would yield these experimental curves (see Supporting Information Section 7). The values for the association constants $K_{M\text{-}D}$ and $K_{MD\text{-}M}$ were then optimized such that the spectra for the three individual species, as extracted from multiple different sets of three experimental curves, were most alike. The resulting UV−vis spectra (for optimized values of $K_{M\text{-}D} = 1 \times 10^4$ M^{-1} and $K_{MD\text{-}M} = 3 \times 10^6$ M^{-1}) of each pure species **M**, $\mathbf{M_2D}$, and **MD**, are shown in Figure 2d. Figure 2e shows the fractions of the macrocycle in the unbound macrocycle **M**, and as a component in $\mathbf{M_2D}$ and **MD** as a function of DABCO concentration, taking into account the obtained association constants. By combining these spectra for the individual species in Figure 2d and the fractions in Figure 2e, UV−vis spectra for the different macrocycle-to-DABCO ratios were reconstructed (Figure 2f), and these were then validated by comparison with the experimentally obtained curves in Figure 2a. Figures 2a,f are in good agreement (see Supporting Information Figure S8a,b for the complete set of UV−vis spectra). The analysis of the UV−vis spectra reveals that **M** is the species of major abundance when [**D**] ≪ [**M**], at increasing concentration of DABCO $\mathbf{M_2D}$ is formed, and **MD** becomes the dominating species when [**D**] ≫ [**M**]. In the presence of 20 mol equiv of DABCO the fraction of **M** residing in $\mathbf{M_2D}$ complex rises to 75%, whereas the fraction of **M** present in **MD** is almost 70% in the presence of 1000 mol equiv of DABCO. The association constant $K_{M\text{-}D}$ is in good agreement with the data for the binding of DABCO to the porphyrin macrocycle without OH groups, obtained from NMR titrations in a 1:1 chloroform/acetonitrile mixture ($c_{porphyrin}$ = 1 mM, $K = 5 \times 10^4$ M^{-1}, in which only 1:1 complex formation was observed).[21]

We further analyzed complex formation with NMR spectroscopy; despite the fact that the concentration used for the ^{1}H NMR analysis ([**M**] = 1.4 mM in $CDCl_3$) is higher than that of interest for the threading studies (see below). The two β-pyrrole proton signals of **M** (at 9.1 and 8.9 ppm) showed a typical upfield shift (to 8.6 and 8.3 ppm, respectively) upon the addition of DABCO, indicating coordination of the ligand to the porphyrin roof (see Supporting Information Figure S10). Furthermore, a characteristic peak below −5 ppm, arising from six methylene protons of the DABCO residing between two

DOI: 10.1021/jacs.5b00431
J. Am. Chem. Soc. 2015, 137, 3915−3923

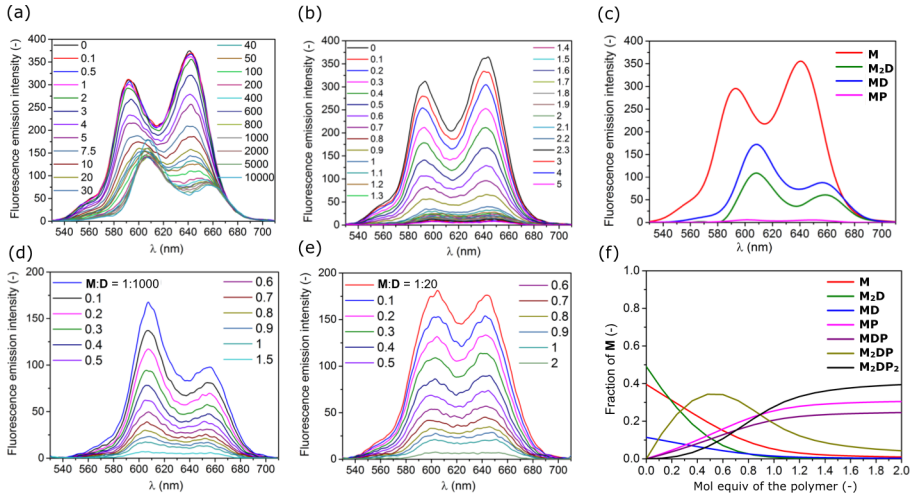

Figure 3. Analysis of the binding between **M**, **D**, and **P** as measured by fluorescence spectroscopy (λ_{ex} = 421 nm, [**M**] = 1 μM in $CHCl_3$, T = 295 K). Mol equiv of the added compounds are indicated. Fluorescence emission spectra of (a) **M** upon addition of **D** and (b) **M** upon addition of **P**. (c) The fluorescence spectra of the individual species extracted from the experimental data and the fractions predicted by the mass-balance model. (d) **MD** (**M**:**D** = 1:1000) upon addition of **P**. (e) $\mathbf{M_2D}$ (**M**:**D** = 1:20) upon addition of **P**. (f) Fraction of the macrocycle within the different complexes as a function of mol equiv of the polymer in the presence of 20 mol equiv of DABCO.

porphyrin cages, indicates the formation of an $\mathbf{M_2D}$ complex. The formation of the **MD** complex in the presence of excess DABCO (4 mol equiv) was not observed. Based on the equilibrium constants derived above, indeed much higher concentrations of DABCO would be required in order to obtain significant amounts of **MD** so that it can be detected by NMR (*vide infra*, Figure 5).

After the evaluation of the binding equilibria between **M** and **D**, we analyzed the binding of polymer **P** to the macrocycle by UV−vis spectroscopy. The Soret band of **M** displayed a typical red shift (7 nm) as a result of binding of 1 mol equiv of viologen in the cavity of the host, resulting in formation of a 1:1 **MP** complex ([**M**] = 5.5 μM in $CHCl_3$) (see Supporting Information Figure S11a). Binding experiments performed with complexes $\mathbf{M_2D}$ (50 mol equiv of DABCO) and **MD** (1000 mol equiv of DABCO) under identical conditions resulted in a slight red shift of the Soret band, which suggests the formation of DABCO-containing polymer-threaded complexes $\mathbf{M_2DP}$, $\mathbf{M_2DP_2}$, and **MDP** (see Supporting Information Figure S11b,c). The absorption maxima of these complexes were hardly distinguishable from those of $\mathbf{M_2D}$, **MD**, and **MP** by UV−vis spectroscopy. Therefore, we continued our binding studies with fluorescence spectroscopy and determined the binding constants from the titration curves obtained using that technique.

Fluorescence spectroscopy is a tool that is commonly used to analyze the interaction of porphyrin receptors with various acceptor compounds, e.g., viologen derivatives.[30] Previous studies have shown that the binding of viologen derivatives inside the porphyrin macrocycle results in the quenching of the fluorescence emission of the porphyrin, and the fraction of porphyrin-viologen complexes in the mixture can be quantified by the decrease in fluorescence intensity.[23,24] Hence, we decided to analyze the binding behavior of the polymer through the cavities of the dimeric system, $\mathbf{M_2D}$, by fluorescence spectroscopy. We first evaluated the binding equilibria between macrocycle (**M**) and DABCO (**D**) in the absence of polymer. The fluorescence emission of **M** was measured upon addition of DABCO ([**M**] = 1 μM in $CHCl_3$, T = 295 K, λ_{ex} = 421 nm). The intensity of the fluorescence signal slightly decreased (20% quenching in the presence of 3 mol equiv of DABCO) during the course of addition, while a red shift (from 641 to 651 nm) and a change in the shape of the fluorescence signal were observed as a result of DABCO coordination to the zinc ion of the macrocycle (Figure 3a). A similar fluorescence titration was performed between macrocycle **M** and polymer **P** in the absence of DABCO under identical conditions. Upon addition of the polymer the intensity of the fluorescence signal of **M** decreased and 95% quenching was observed in the presence of 1 mol equiv of polymer (Figure 3b). This suggests that the majority of the macrocycle is threaded by the polymer forming a 1:1 **MP** complex.[24,31] We extracted the fluorescence spectra and the fraction of each possibly formed species, i.e., **M**, $\mathbf{M_2D}$, **MD**, and **MP**, from Figure 3a,b by using the binding model described in Figure 2c (see Supporting Information Section 10) and reconstructed the individual fluorescence spectra by combining these data. The spectra of the individual species depicted in Figure 3c indicate that the reconstructed fluorescence spectrum of **M** is in good agreement with that of the experimental fluorescence spectrum and the spectra of the different species (**M**, $\mathbf{M_2D}$, **MD** and **MP**) indeed overlap. Furthermore, the polymer-threaded 1:1 complex, **MP**, hardly contributes to the fluorescence signal. The association constants, $K_{\mathbf{M\text{-}D}} = 1.5 \times 10^4$ M^{-1} and $K_{\mathbf{MD\text{-}M}} = 5 \times 10^6$ M^{-1}, could be obtained for DABCO-macrocycle binding by fitting the fluorescence curves in Figure 3a with the model (see Supporting Information Section 10.1). These association constants are slightly higher than those obtained from the UV−vis curves above, however, they still lie in the valley of the contour plot obtained for the UV−vis titration data (*vide supra*, see Supporting Information Section 7 and Figure S6) and thus fit both experiments. The slight difference may be due to deviations in the used exact experimental concentrations of the mixtures during the UV−vis and fluorescence measurements. The association constant derived for the binding of the polymer in the macrocycle in the absence of DABCO is calculated to be $K_{\mathbf{M\text{-}P}} = 3 \times 10^7$ M^{-1} (see Supporting Information Section 10.2).

After analyzing the binding equilibria between **M**-**D** and **M**-**P**, respectively, we studied the binding behavior of the polymer to the complexes **MD** and $\mathbf{M_2D}$ by performing titration

DOI: 10.1021/jacs.5b00431
J. Am. Chem. Soc. 2015, 137, 3915−3923

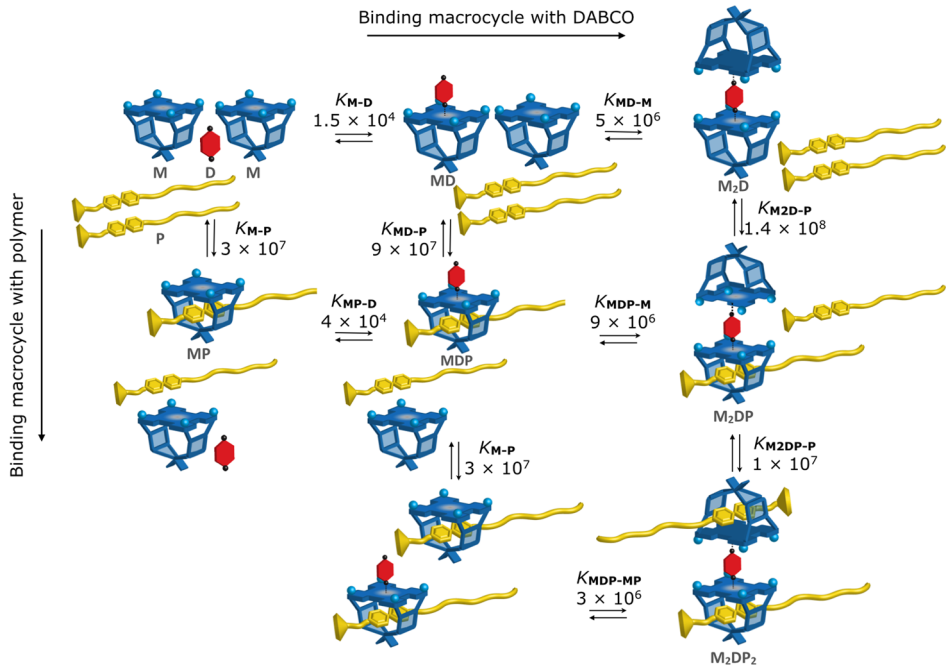

Figure 4. Binding scheme showing all possible complexes and equilibria involving **M**, **D**, and **P**, with the corresponding association constants.

experiments under identical conditions. Upon addition of 1 mol equiv of polymer to **MD** (**M**:**D** = 1:1000, in which the **MD** complex is present in majority) the polymer is threaded through the cavity of the **MD**, and **MDP** is formed exclusively, which results in the almost complete quenching of the fluorescence signal (Figure 3d). Next, the polymer was added to the **M**-**D** mixture (**M**:**D** = 1:20) in which the dimeric $\mathbf{M_2D}$ complex is present in majority. During the course of polymer addition the intensity of the fluorescence signal decreased, suggesting the threading of the polymer through the cavities of the complexes to form $\mathbf{M_2DP}$ and $\mathbf{M_2DP_2}$. In the presence of 1 mol equiv of polymer the fluorescence emission signal was also almost completely quenched; however, the amount of quenching is slightly less than that of **MD**, which is presumably due to the fact that one cavity in $\mathbf{M_2DP}$ is left partly unoccupied.(Figure 3e). During the titration of $\mathbf{M_2D}$ with polymer, a two-step process for the binding of the polymer to each cavity was not observed in the titration curve (see Supporting Information Figure S15c). Apparently, $\mathbf{M_2DP}$ and $\mathbf{M_2DP_2}$ are formed simultaneously. In order to distinguish the species formed during the titration we based our analysis on the combination of multiple spectra, and we did not assess them at a single wavelength but on the basis of complete spectra. We will provide further Supporting Information on the binding behavior of polymers to $\mathbf{M_2D}$ with phase diagrams in the next section (*vide infra* Figure 5a,b).

The interpretation of the fluorescence data was performed in a similar fashion as for the UV−vis curves described in the previous section. In the presence of three components, **M**, **P**, and **D**, multiple interactions take place, and the spectra of the different complexes overlap. The fluorescence spectra for the titration of polymer **P** into solutions containing **M**−**D** complexes were analyzed by taking into account the additional binding constants for the formation of **MDP**, $\mathbf{M_2DP}$, and $\mathbf{M_2DP_2}$ and their contributions to the fluorescence signals. For each mixture, theoretical fluorescence spectra were calculated by using the fraction of species determined by the mass-balance model and the spectra of the individual species shown in Figure 3c. Assuming that the contribution of **MDP** to the fluorescence signal is very small as was the contribution of **MP**, the association constant $K_{\mathbf{MP\text{-}D}}$ (= 4 × 10^4 M^{-1}) could be determined (see Supporting Information Section 10.3 and Figure S14). The association constant of **D** to **M** in the presence of polymer is almost 3 times larger than that in the absence of polymer ($K_{\mathbf{M\text{-}D}}$ = 1.5 × 10^4 M^{-1}) as a result of allosteric effects as observed earlier for the binding of dimethylviologen to the porphyrin cavity in the presence of DABCO.[21] Similarly the association constant of the polymer to **M** shows a 3-fold increase in the presence of **D** ($K_{\mathbf{M\text{-}P}}$ = 3 × 10^7 M^{-1} and $K_{\mathbf{MD\text{-}P}}$ = 9 × 10^7 M^{-1}). Assuming that the contributions of all polymer-threaded macrocycles to the fluorescence signal are equally small and the contribution of the unoccupied macrocycle in $\mathbf{M_2DP}$ to the fluorescence signal is equal to that of one macrocycle in $\mathbf{M_2D}$, the association constants for $K_{\mathbf{MDP\text{-}M}}$ (= 9 × 10^6 M^{-1}) and $K_{\mathbf{MDP\text{-}MP}}$ (= 3 × 10^6 M^{-1}) could be determined from the fluorescence spectra of the **M**:**D** mixture (**M**:**D** = 1:20) (see Supporting Information Section 10.3 and Figure S15). This implies that the association constant for the binding of the polymer in one of the cavities of $\mathbf{M_2D}$ to form $\mathbf{M_2DP}$, $K_{\mathbf{M_2D\text{-}P}}$ (= 1.4 × 10^8 M^{-1}) is larger than that for the binding of the polymer in the cavity of **MD** to form **MDP** $K_{\mathbf{MD\text{-}P}}$ (= 9 × 10^7 M^{-1}), whereas the association constant of the second polymer to the vacant cavity of $\mathbf{M_2DP}$ in order to form the pentameric complex, $\mathbf{M_2DP_2}$, is smaller ($K_{\mathbf{M_2DP\text{-}P}}$ = 1 × 10^7 M^{-1}). Hence, the association constant for the binding of the second polymer to form the pentameric complex, $K_{\mathbf{M_2DP\text{-}P}}$, is not the largest association constant in the system. This does not mean, however, that the fraction of $\mathbf{M_2DP_2}$ is the lowest in solution, since the fraction of a species cannot be extracted from a single equilibrium (constant) but only from the complete mass-balance of the system (Figure 4). The presence of significant amounts of the pentameric complex, $\mathbf{M_2DP_2}$, relative to **MDP**, depends on whether the ratio $[\mathbf{M_2DP_2}]/[\mathbf{MDP}] = K_{\mathbf{MDP\text{-}MP}} \times K_{\mathbf{M\text{-}P}} \times [\mathbf{M}] \times [\mathbf{P}]$ is larger or smaller than 1, which is also dependent on all other association

DOI: 10.1021/jacs.5b00431
J. Am. Chem. Soc. 2015, 137, 3915−3923

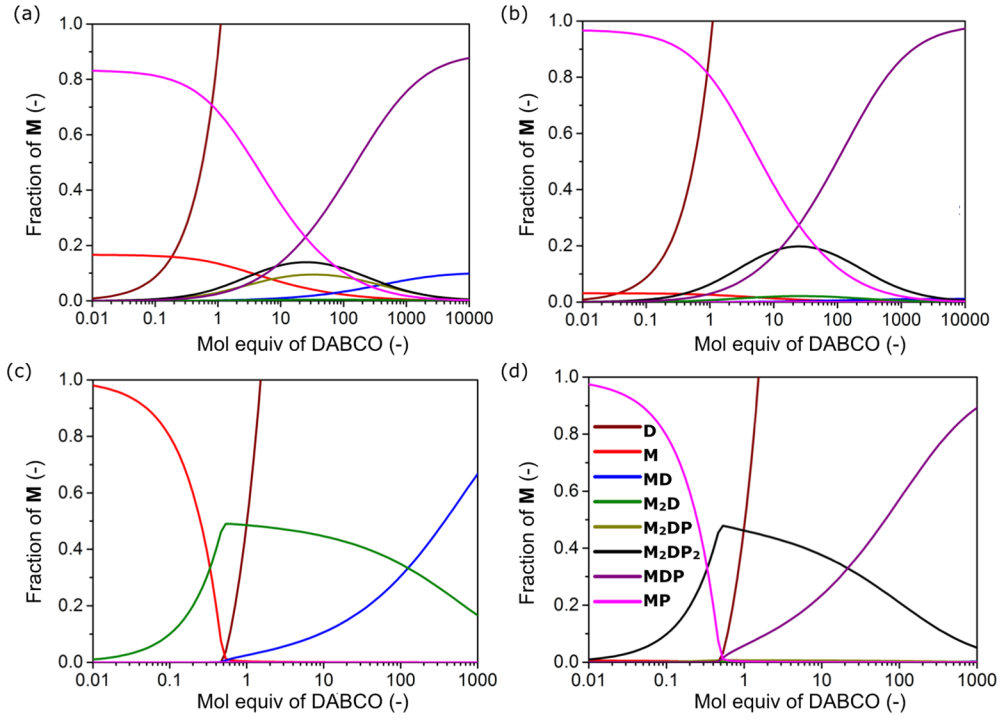

Figure 5. Calculated fractions of the macrocycle within different species as a function of mol equiv of DABCO under various conditions based on the association constants obtained from fluorescence titration experiments. (a) [**M**] = 1 μM and [**P**] = 1 μM. (b) [**M**] = 1 μM and [**P**] = 2 μM. (c) [**M**] = 1 mM, in the absence of polymer. The concentration of **M** present in the form of $\mathbf{M_2DP}$ (dark yellow line), $\mathbf{M_2DP_2}$ (black line), **MDP** (purple line), and **MP** (magenta line) is very low in the absence of polymer. (d) [**M**] = 1 mM, in the presence of polymer, [**P**] = 1 mM. Under these conditions the equilibrium is directed to the full assembly of $\mathbf{M_2DP_2}$, therefore the fractions of **M** present in the form of $\mathbf{M_2DP}$, $\mathbf{M_2D}$, **MD** are close to 0 in the plot.

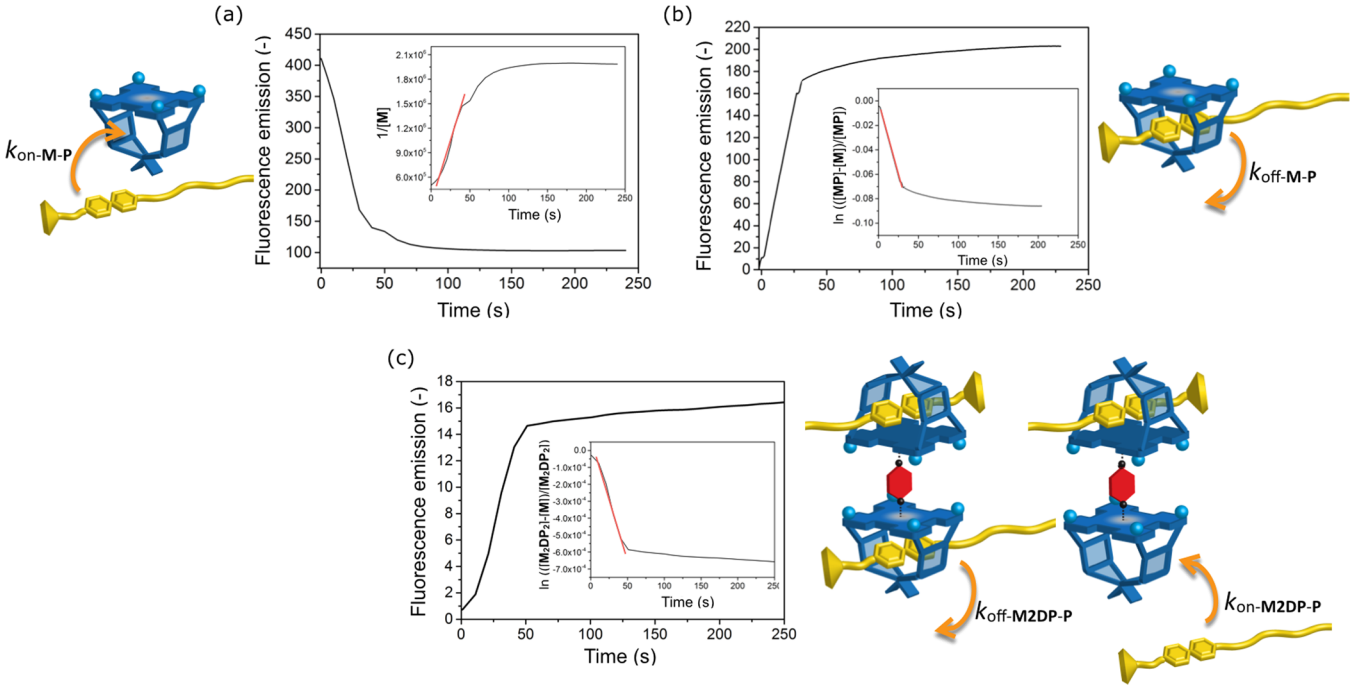

Figure 6. Threading studies. Fluorescence emission as a function of time. (a) Threading of **P** (1 mol equiv) through **M**. [**M**] = 2 μM. (b) Dethreading of **P** from **MP**. Starting from [**M**] = 1 mM, [**P**] = 1 mM to 1 μM concentration. (c) Dethreading of **P** from $\mathbf{M_2DP_2}$. Starting from [**M**] = 1 mM, [**D**] = 0.5 mM, [**P**] = 1 mM to μM concentration. Monitored at 649 nm. The insets are fits (red lines), which are obtained from first-order (dethreading) and second-order (threading) rate laws.

constants since [**M**] and [**P**] are the free macrocycle and free polymer concentrations that are present in the solution, determining the whole mass-balance (see Supporting Information Section 5, equations for [$\mathbf{M_2DP_2}$] and [**MDP**]). The calculated fraction of **M** residing in the various complexes as a function of the polymer concentration in the presence of 20

DOI: 10.1021/jacs.5b00431
J. Am. Chem. Soc. 2015, 137, 3915−3923

mol equiv of DABCO is shown in Figure 3f. In the presence of 2 mol equiv of polymer, the concentration of $\mathbf{M_2DP_2}$ is 0.2 μM, which indicates that 40% of the macrocycle is present in the form of the pentameric complex (i.e., in the presence of at least 1 mol equiv of polymer, the highest fraction of the macrocycle is present in $\mathbf{M_2DP_2}$). As a result of allosteric interactions between the macrocyclic host, the DABCO ligand and the viologen-functionalized polymer guest, the polymer-threaded double-decker macrocycle complex is formed as the major species at these dilute concentrations.

Using the above derived association constants, the concentration of the macrocycle residing in each species was also calculated as a function of the DABCO concentration for different conditions (Figure 5). It is clearly represented in Figure 5a that $\mathbf{M_2DP}$ (dark yellow line) is present in solution when [**D**] = 20 μM and [**P**] = 1 μM, while the assembly is fully directed toward $\mathbf{M_2DP_2}$ (black line) when [**D**] = 20 μM and [**P**] = 2 μM (Figure 5b). Under concentrated conditions when [**M**] = 1 mM and [**D**] = 0.5 mM and in the absence of polymer, $\mathbf{M_2D}$ (green line) is the complex of major abundance, while **MD** is predicted to become the majority complex in the presence of excess DABCO (>100 mol equiv) in solution (Figure 5c). Furthermore, the fraction of $\mathbf{M_2DP_2}$ is almost 100% when [**D**] = 0.5 mM and [**P**] = 1 mM (Figure 5d). These phase diagrams showing the precise distribution of the species will be useful for the (de)threading kinetics described in the next section.

Kinetics of Polymer Threading through the Macrocyclic Dimers. After having analyzed the thermodynamics of the binding of the polymer **P** to the double-cage $\mathbf{M_2D}$ system, we studied the threading and dethreading kinetics of this polymer through the cavities in $\mathbf{M_2D}$ and compared these with those of the single-cage, monomeric system **M**. First, we determined the threading rate constant of the polymer through unbound macrocycle **M**, which is more straightforward since only two components **M** and **P** are present. To a known volume of macrocycle **M** ([**M**] = 2 μM in $CHCl_3$), 1.0 mol equiv of polymer solution was added at 295 K, and the fluorescence emission intensity of **M** was measured as a function of time. The fluorescence intensity decreased over time, indicating that the macrocycle finds the open end of the polymer and threads onto the polymer chain, eventually reaching the viologen trap, upon which the fluorescence of the porphyrin is quenched (Figure 6a).[23,24] The rate of threading follows second-order kinetics, thus the slope of the plot of 1/[**M**] against time gives the threading rate constant, $k_{\text{on-M-P}}$ (inset of Figure 6a).[23] The fits revealed that the threading rate of the polymer through macrocycle **M** ($k_{\text{on-M-P}} = 3.4 \times 10^4$ M^{-1} s^{-1}) is similar to the value determined previously in $CHCl_3$/CH_3CN (1:1, v/v) solution ($k_{\text{on-M-P}} = 4.1 \times 10^4$ M^{-1} s^{-1} for a longer polymer chain, repeating unit, n = 18).[24] The dethreading rate of the polymer from **MP** was measured by adding a known amount of a concentrated solution of the complex in $CHCl_3$ ([**MP**] = 1 mM, **M**:**P** in **MP** = 1:1) to $CHCl_3$ (2 mL) and measuring the increase in the fluorescence emission over time (Figure 6b). Upon dilution (from 1 mM to 1 μM), the polymer and the macrocycle partly dissociate, and a new equilibrium is reached. Previous studies showed that the dethreading is a first-order process, thus the slope of ln(([**MP**] − [**M**])/[**MP**]) against time gives the $-k_{\text{off}}$ value (inset of Figure 6b)[23] which means that $k_{\text{off}} = 2.3 \times 10^{-3}$ s^{-1} for the dethreading of **P** from **MP** (Table 1). The association constant ($K_{\text{M-P}} = 1.5 \times 10^7$ M^{-1}) obtained from the ratio of k_{on} and k_{off} is of the same order of magnitude as the $K_{\text{M-P}}$ value of 3×10^7 M^{-1} obtained above.

Table 1. Calculated Threading and Dethreading Rate Constants for MP And $\mathbf{M_2DP_2}$ as Determined by the First- and Second-Order Reaction Rate Laws, Respectively

complex	k_{on} (M^{-1} s^{-1})	k_{off} (s^{-1})	k (M^{-1})
MP	3.4×10^4	2.3×10^{-3}	$K_{\text{M-P}} = 1.5 \times 10^7$
$\mathbf{M_2DP_2}$	1.3×10^2	$\leq 1.3 \times 10^{-5}$	$K_{\text{M2DP-P}} = 1.0 \times 10^7$

Next, we studied the threading and dethreading kinetics of the polymer in and out of the $\mathbf{M_2D}$ complex. As shown in Figure 2e, the dimeric complex, $\mathbf{M_2D}$, is not the only species in solution when [**D**] = 20 μM and [**M**] = 1 μM (the fraction of **M** in $\mathbf{M_2D}$ is 70%, in **MD** is 15%, and in the unbound form, **M**, is 15%). Therefore, the threading rate constant of the polymer through $\mathbf{M_2D}$ ($k_{\text{on-M2D-P2}}$) cannot be measured directly. Instead, we derived the threading rate constant of one polymer through the unoccupied cavity in $\mathbf{M_2DP}$ from the association constant, $K_{\text{M2DP-P}}$. In order to do that, we first determined the dethreading rate constant of the polymer from one of the cavities in $\mathbf{M_2DP_2}$ to form $\mathbf{M_2DP}$ ($k_{\text{off-M2DP2}}$). Subsequently, we calculated the threading rate constant of the polymer through the unoccupied cavity of $\mathbf{M_2DP}$ ($k_{\text{on-M2DP-P}}$) using the already known association constant $K_{\text{M2DP-P}}$ (= $k_{\text{on}}/k_{\text{off}}$). A known amount of a concentrated solution of the $\mathbf{M_2DP_2}$ complex in $CHCl_3$ ([$\mathbf{M_2DP_2}$] = 1 mM, **M**:**D**:**P** = 1:0.5:1; the fraction of **M** in $\mathbf{M_2DP_2}$ in the mixture is almost 100% when [**M**] = 1 mM, [**D**] = 0.5 mM, and [**P**] = 1 mM, as shown in Figure 5d) was diluted in $CHCl_3$ (2 mL), and the increase in the fluorescence emission was measured over time (Figure 6c). Upon dilution to 1 μM concentration, the pentameric complex dissociates, and a new equilibrium is reached with a new composition, which is mainly **MP** and **M** (the equilibrium is shifted from the assembly state presented in Figure 5d to the one in Figure 5a). Figure 5a shows that in the new composition $\mathbf{M_2DP}$ (which contains 4% of the total macrocycle concentration) is still included in the solution when [**M**] = 1 μM, [**D**] = 0.5 μM and [**P**] = 1 μM, suggesting that the new equilibrium is reached via the $\mathbf{M_2DP}$ complex. The dethreading of one polymer from one of the cavities in $\mathbf{M_2DP_2}$ leads to the formation of $\mathbf{M_2DP}$ and **P**, which further dissociates to **MDP**, **M**, and **P** in solution (*vide supra*, Figure 4). The rate constant of dethreading of **P** from $\mathbf{M_2DP_2}$ was calculated by fitting the experimental data as described above giving the value of $k_{\text{off-M2DP-P}} = 1.3 \times 10^{-5}$ s^{-1} (Table 1). It should be noted that the dissociation of $\mathbf{M_2DP_2}$ to **MP** and **M** can also occur via the splitting of $\mathbf{M_2DP_2}$ to **MDP** and **MP**, which further dissociates to **MDP**, **M**, and **P** (*vide supra*, Figure 4). This would mean that the dethreading rate of the polymer from $\mathbf{M_2DP_2}$ to form $\mathbf{M_2DP}$ is even slower than that of the splitting (i.e., the formation of $\mathbf{M_2DP}$ is not the favored pathway) and that the dethreading rate constant of the polymer from $\mathbf{M_2DP_2}$ would result in even a lower value than 1.3×10^{-5} s^{-1}.

The dethreading rate constant of the polymer from $\mathbf{M_2DP_2}$, $k_{\text{off-M2DP-P}}$, is remarkably smaller than that of the polymer from **MP**, $k_{\text{off-M-P}}$, suggesting that the polymer is held within the cavity of the macrocycle in the pentameric complex $\mathbf{M_2DP_2}$ much stronger as a result of allosteric interactions between the host, the guest, and the ligand. This leads to a very slow

DOI: 10.1021/jacs.5b00431
J. Am. Chem. Soc. 2015, 137, 3915−3923

dissociation rate of the polymer from the complex. The threading rate constant of the polymer through the unoccupied cavity of **M_2DP** obtained from the corresponding association constant, $K_{M_2DP\text{-}P}$ (= k_{on}/k_{off}), is also very low ($k_{on\text{-}M_2DP\text{-}P}$ = 1.3 × 10^2 M^{-1} s^{-1}) compared to $k_{on\text{-}M\text{-}P}$ (= 3.4 × 10^4 M^{-1} s^{-1}). This may be due to the occupation of the second cavity by the open end of the already threaded polymer. Previous studies on the mechanism of polymer threading revealed that the threading may follow either an intermolecular or intramolecular pathway.[24] In the former case the macrocycle finds the open end of the polymer chain and threads on it, while during an intramolecular pathway the polymer first interacts with the outside of the macrocycle and subsequently threads on it. The formation of a viologen−macrocycle complex on the outside of the host enhances the chance of loop formation, facilitating the threading of the open end of the polymer chain through the cavity of the host. In this case the threading rate is dependent on the effective molarity of the reactive components, which are, the cavity and the open end of the chain. Similarly, in a dimeric **M_2DP** system, the open end of the polymer chain residing in one cavity may block the second cavity via a looping mechanism, thereby delaying the threading of a second polymer through this cavity (Figure 7). The remarkably slow threading

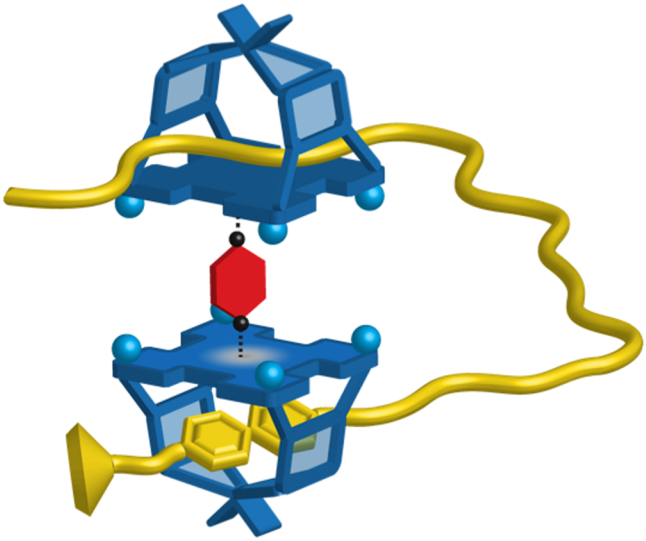

Figure 7. Schematic representation of the macrocyclic dimer in which the second cavity is blocked by the open end of the polymer residing in the first cavity.

and dethreading rates of a polymer through and from a dimeric system suggest that there is a communication between the two cages via interactions, that may be partly allosteric in nature, between macrocyclic host, ligand DABCO, and polymeric guest.

CONCLUSIONS

We have studied the thermodynamics and kinetics of the binding process of a viologen-substituted polymer to a dimeric complex consisting of two zinc porphyrin macrocycles bridged by a DABCO ligand. The binding of the polymer to the cavities of the dimer leads to a complex system of species in solution. We analyzed the binding equilibria of the various polymer−macrocycle−ligand combinations by UV−vis and fluorescence spectroscopy. We provided a methodology to quantify the precise fractions of each species formed in the binding process by separating the spectral data that overlap. Using this methodology we were able to determine the association constants of all complexes that are formed in solution. It is shown that the 2:1 porphyrin macrocycle−DABCO complex is formed even under very dilute conditions. The viologen-substituted polymer can then be threaded through the cavities of this dimeric system, giving rise to a pentameric complex **M_2DP_2**, exclusively. We have studied the kinetics of the polymer threading in this pentameric system and compared this with that of the free macrocycle **M**. The enhanced binding affinity of the polymer as a result of allosteric interactions between the host, ligand, and guest in the pentameric complex led to a very slow dethreading of the polymer from **M_2DP_2**. More importantly, also a very slow rate was observed for the threading of the polymer through **M_2DP** to form **M_2DP_2**, which might be the result of the looping of the open end of the polymer bound in the first cavity through the unoccupied cavity, delaying the threading of the second polymer.

The obtained results are valuable for the construction of the molecular Turing machine mentioned in the Introduction section. The data represented here show that information transfer is possible between two self-assembled cage molecules, both with respect to the thermodynamics of the binding process and the kinetics of the threading and dethreading processes. The next step is to combine the observed cooperative effects with function, e.g., catalysis. To this end the zinc center of the porphyrin will be replaced by a manganese center, which is known to lead to a good epoxidation catalyst.[32,33] One of the goals is to transfer information, e.g., from a chiral polymeric guest (polyamino acid) threaded in one of the porphyrin cages, to a polymer chain containing double bonds (polybutadiene) that resides in the second cage. Such an information transfer may result in a "writing" process, in which oxygen atoms in the form of epoxides are positioned along the polybutadiene chain by an allosteric catalytic reaction, which copies the absolute configuration of the chiral polymeric guest. Work along this line is in progress.

ASSOCIATED CONTENT

Supporting Information

General experimental protocols, ^{1}H NMR, additional UV−vis and fluorescence measurements. Details of the mass-balance model and the applications of the model. Additional reconstructed UV−vis and fluorescence emission spectra. This material is available free of charge via the Internet at http://pubs.acs.org.

AUTHOR INFORMATION

Corresponding Authors

*scantekin@gmail.com
*r.nolte@science.ru.nl

Notes

The authors declare no competing financial interest.

ACKNOWLEDGMENTS

This research was supported by the European Research Council in the form of an ERC Advanced grant to R.J.M.N. (ALPROS-290886) and an ERC Starting grant to J.A.A.W.E (NANOCAT-259064). Further financial support was obtained from the Council for the Chemical Sciences of The Netherlands

DOI: 10.1021/jacs.5b00431
J. Am. Chem. Soc. 2015, 137, 3915−3923

Organization for Scientific Research (CW-NWO) (Vidi grant for J.A.A.W.E and Vici grant for A.E.R) and from the Ministry of Education, Culture, and Science (Gravity program 024.001.035). We would like to thank Theo Peters for his help with the synthesis of the macrocycle, L. Pitet for his help with the synthesis of the viologen-substituted polymer and the art work, and S. Varghese for useful discussions.

REFERENCES

(1) Kremer, C.; Lutzen, A. *Chem.—Eur. J.* **2013**, *19*, 6162.
(2) Asakawa, M.; Iqbal, S.; Stoddart, J. F.; Tinker, N. D. *Angew. Chem. Int. Ed.* **1996**, *35*, 976.
(3) Oliveri, C. G.; Gianneschi, N. C.; Nguyen, S. T.; Mirkin, C. A.; Stern, C. L.; Wawrzak, Z.; Pink, M. *J. Am. Chem. Soc.* **2006**, *128*, 16286.
(4) Kuwabara, J.; Yoon, H. J.; Mirkin, C. A.; DiPasqualeb, A. G.; Rheingold, A. L. *Chem. Commun.* **2009**, 4557.
(5) Yoon, H. J.; Kuwabara, J.; Kim, J.-K.; Mirkin, C. A. *Science* **2010**, *330*, 66.
(6) Mendez-Arroyo, J.; Barroso-Flores, J.; Lifschitz, A. M.; Sarjeant, A. A.; Stern, C. L.; Mirkin, C. A. *J. Am. Chem. Soc.* **2014**, *136*, 10340.
(7) McGuirk, C. M.; Stern, C. L.; Mirkin, C. A. *J. Am. Chem. Soc.* **2014**, *136*, 4689.
(8) Ramsay, W. J.; Nitschke, J. R. *J. Am. Chem. Soc.* **2014**, *136*, 7038.
(9) Traylor, T. G.; Mitchell, M. J.; Ciconene, J. P.; Nelson, S. *J. Am. Chem. Soc.* **1982**, *104*, 4986.
(10) Tabushi, I.; Sasaki, T. *J. Am. Chem. Soc.* **1983**, *105*, 2901.
(11) Rebek, J.; Costello, T.; Marshall, L.; Wattley, R.; Gadwood, R. C.; Onan, K. *J. Am. Chem. Soc.* **1985**, *107*, 7481.
(12) Ayabe, M.; Ikeda, A.; Kubo, Y.; Takeuchi, M.; Shinkai, S. *Angew. Chem., Int. Ed.* **2002**, *41*, 2790.
(13) Takeuchi, M.; Imada, T.; Shinkai, S. *J. Am. Chem. Soc.* **1996**, *118*, 10658.
(14) Thordarson, P.; Bijsterveld, E. J. A.; Elemans, J. A. A. W.; Kasak, P.; Nolte, R. J. M.; Rowan, A. E. *J. Am. Chem. Soc.* **2003**, *125*, 1186.
(15) Sato, H.; Tashiro, K.; Shinmori, H.; Osuka, A.; Aida, T. *Chem. Commun.* **2005**, *18*, 2324.
(16) Rebek, J.; Wattley, R. V. *J. Am. Chem. Soc.* **1980**, *102*, 4853.
(17) Al-Sayah, M. H.; Branda, N. R. *Angew. Chem., Int. Ed.* **2000**, *39*, 945.
(18) Tobey, S. L.; Anslyn, E. V. *J. Am. Chem. Soc.* **2003**, *125*, 10963.
(19) Taylor, P. N.; Anderson, H. L. *J. Am. Chem. Soc.* **1999**, *121*, 11538.
(20) Deutman, A. B. C.; Monnereau, C.; Moalin, M.; Coumans, R. G. E.; Veling, N.; Coenen, M.; Smits, J. M. M.; de Gelder, R.; Elemans, J. A. A. W.; Ercolani, G.; Nolte, R. J. M.; Rowan, A. E. *Proc. Natl. Acad. Sci. U.S.A.* **2009**, *106*, 10471.
(21) Thordarson, P.; Coumans, R. G. E.; Elemans, J. A. A. W.; Thomassen, P. J.; Visser, J.; Rowan, A. E.; Nolte, R. J. M. *Angew. Chem., Int. Ed.* **2004**, *43*, 4755.
(22) Coumans, R. G. E.; Elemans, J. A. A. W.; Rowan, A. E.; Nolte, R. J. M. *Chem.—Eur. J.* **2013**, *19*, 7758.
(23) Coumans, R. G. E.; Elemans, J. A. A. W.; Nolte, R. J. M.; Rowan, A. E. *Proc. Natl. Acad. Sci. U.S.A.* **2006**, *103*, 19647.
(24) Deutman, A. B. C.; Monnereau, C.; Elemans, J. A. A. W.; Ercolani, G.; Nolte, R. J. M.; Rowan, A. E. *Science* **2008**, *322*, 1668.
(25) Elemans, J. A. A. W.; Claase, M. B.; Aarts, P. P. M.; Rowan, A. E.; Schenning, A. P. H. J.; Nolte, R. J. M. *J. Org. Chem.* **1999**, *64*, 7009.
(26) Mak, C. C.; Bampos, N.; Sanders, J. K. M. *Angew. Chem., Int. Ed.* **1998**, *37*, 3020.
(27) Hunter, C. A.; Tregonning, R. *Tetrahedron* **2002**, *58*, 691.
(28) Ballester, P.; Costa, A.; Castilla, A. M.; Deya, P. M.; Frontera, A.; Gomila, R. M.; Hunter, C. A. *Chem.—Eur. J.* **2005**, *11*, 2196.
(29) Ballester, P.; Hunter, C. A. *J. Am. Chem. Soc.* **2006**, *128*, 5560.
(30) Yagi, S.; Ezoe, M.; Yonekura, I.; Takagishi, T.; Nakazumi, H. *J. Am. Chem. Soc.* **2003**, *125*, 4068.
(31) Deutman, A. B. C.; Cantekin, S.; Elemans, J. A. A. W.; Rowan, A. E.; Nolte, R. J. M. *J. Am. Chem. Soc.* **2014**, *136*, 9165.
(32) Thordarson, P.; Bijsterveld, E. J. A.; Rowan, A. E.; Nolte, R. J. M. *Nature* **2003**, *424*, 915.
(33) Elemans, J. A. A. W.; Bijsterveld, E. J. A.; Rowan, A. E.; Nolte, R. J. M. *Chem. Commun.* **2000**, 2443.

DOI: 10.1021/jacs.5b00431
J. Am. Chem. Soc. 2015, 137, 3915−3923